Effects of acute Rho kinase inhibition on chronic hypoxia-induced changes in proximal and distal pulmonary arterial structure and function

Rebecca R. Vanderpool, Ah Ram Kim, Robert Molthen and Naomi C. Chesler

J Appl Physiol 110:188-198, 2011. First published 18 November 2010;
doi:10.1152/japplphysiol.00533.2010

J Appl Physiol 110: 188–198, 2011.
First published November 18, 2010; doi:10.1152/japplphysiol.00533.2010.

Effects of acute Rho kinase inhibition on chronic hypoxia-induced changes in proximal and distal pulmonary arterial structure and function

Rebecca R. Vanderpool,[1] Ah Ram Kim,[1] Robert Molthen,[2] and Naomi C. Chesler[1]

[1]*Department of Biomedical Engineering, University of Wisconsin-Madison, Madison; and* [2]*Department of Medicine-Pulmonary and Critical Care, Medical College of Wisconsin, Milwaukee, Wisconsin*

Submitted 14 May 2010; accepted in final form 11 November 2010

Vanderpool RR, Kim AR, Molthen R, Chesler NC. Effects of acute Rho kinase inhibition on chronic hypoxia-induced changes in proximal and distal pulmonary arterial structure and function. *J Appl Physiol* 110: 188–198, 2011. First published November 18, 2010; doi:10.1152/japplphysiol.00533.2010.—Hypoxic pulmonary hypertension (HPH) is initially a disease of the small pulmonary arteries. Its severity is usually quantified by pulmonary vascular resistance (PVR). Acute Rho kinase inhibition has been found to reduce PVR toward control values in animal models, suggesting that persistent pulmonary vasoconstriction is the dominant mechanism for increased PVR. However, HPH may also cause proximal arterial changes, which are relevant to right ventricular (RV) afterload. RV afterload can be quantified by pulmonary vascular impedance, which is obtained via spectral analysis of pulsatile pressure-flow relationships. To determine the effects of HPH independent of persistent pulmonary vasoconstriction in proximal and distal arteries, we quantified pulsatile pressure-flow relationships before and after acute Rho kinase inhibition and measured pulmonary arterial structure with microcomputed tomography. In control lungs, Rho kinase inhibition decreased 0 Hz impedance (Z_0), which is equivalent to PVR, from 2.1 ± 0.4 to 1.5 ± 0.2 mmHg·min·ml^{-1} ($P < 0.05$) and tended to increase characteristic impedance (Z_C) from 0.21 ± 0.01 to 0.22 ± 0.01 mmHg·min·ml^{-1}. In HPH lungs, Rho kinase inhibition decreased Z_0 ($P < 0.05$) without affecting Z_C. Microcomputed tomography measurements performed on lungs after acute Rho kinase inhibition demonstrated that HPH significantly decreased the unstressed diameter of the main pulmonary artery (760 ± 60 vs. 650 ± 80 μm; $P < 0.05$), decreased right pulmonary artery compliance, and reduced the frequency of arteries of diameter 50–100 μm (both $P < 0.05$). These results demonstrate that acute Rho kinase inhibition reverses many but not all HPH-induced changes in distal pulmonary arteries but does not affect HPH-induced changes in the conduit arteries that impact RV afterload.

pulmonary circulation; Y27632; impedance; arterial biomechanics

PULMONARY ARTERIAL HYPERTENSION is clinically defined as a mean pulmonary arterial pressure (mPAP) >25 mmHg at rest with a pulmonary arterial wedge pressure <15 mmHg (34). While mPAP and a single-point pulmonary vascular resistance calculation (mPAP divided by cardiac output) are the most common metrics of hypertension severity (41), neither is a measure of the pulsatile work required by the right ventricle (RV) to cyclically pump blood to the pulmonary vasculature. Furthermore, increased mPAP alone is not enough to cause RV failure (3). A more effective measure of total RV afterload is the pulmonary vascular impedance (PVZ), which depends on both proximal compliance and distal resistance and is calculated from pulsatile pressure-flow relationships. The clinical importance of proximal compliance has been increasingly recognized (6, 14, 32). Additionally, decreased main pulmonary artery compliance is an excellent predictor of mortality in pulmonary arterial hypertension (14, 32). Therefore, it is important to understand both the proximal and the distal arterial effects of drugs used to treat pulmonary arterial hypertension.

Many drugs efficacious for the treatment of severe pulmonary hypertension do not decrease mPAP or resistance as much as expected given the resulting increases in patient exercise capacity and decreasing mortality (5, 13). It has been speculated that these drugs function by direct action on the RV (i.e., by increasing contractility) and/or by decreasing the pulsatile hydraulic load (61), which depends on proximal compliance (14, 32). An exception is the Rho kinase inhibitor fasudil, which has been found to modestly reduce pulmonary vascular resistance in patients with severe pulmonary hypertension (11), secondary pulmonary hypertension (30), and idiopathic pulmonary hypertension (21). In experimental animals, acute Rho kinase inhibition has been shown to nearly eliminate increases in pulmonary artery pressure induced by chronic hypoxia (19, 43) and is a major contributor to pulmonary hypertension in monocrotaline-injected rats (18, 42) as well as those treated with the vascular endothelial growth factor receptor blocker SUGEN-5416 (46); see Ref. 35 for a comprehensive review. Nevertheless, the effects of Rho kinase inhibition on proximal compliance and pulsatile pressure-flow relationships in the lung remain unknown.

We have previously reported on the utility of the isolated, ventilated, perfused lung system for measuring pulsatile pressure-flow relationships independent of changes in sympathetic nervous system tone, anesthesia, and volume status (60), which cannot be avoided in intact animal preparations. In addition, we have used microcomputed tomography to quantify the changes in proximal and distal arterial morphometry and mechanics that occur with chronic hypoxia-induced hypertension in rats (39). Here, we combine these techniques to determine the effects of acute Rho kinase inhibition on chronic hypoxia-induced changes in RV afterload and proximal and distal pulmonary artery morphometry and mechanics in mice. Given the frequent and increasing use of genetically engineered mice to understand the molecular mechanisms of human disease, techniques appropriate for mouse lungs such as these are vital. We hypothesized that acute Rho kinase inhibition would eliminate persistent distal vasoconstriction, thereby normalizing mPAP and pulmonary vascular resistance, but that proximal arterial stiffening—and subsequent changes in PVZ—would persist.

METHODS

Animal handling. Twenty-four male 10- to 12-wk-old C57BL6/J mice, 25.8 ± 2.3 g body wt, were used (Jackson Laboratory, Bar Harbor, ME). Mice were exposed at the University of Wisconsin-

Address for reprint requests and other correspondence: N. C. Chesler, Univ. of Wisconsin at Madison, 2146 Engineering Centers Bldg., 1550 Engineering Drive, Madison, WI 53706-1609 (e-mail: chesler@engr.wisc.edu).

Madison Biotron facility to zero [control (CTL): $n = 14$] or 10 days [hypoxic pulmonary hypertension (HPH): $n = 10$] of hypobaric hypoxia such that the partial pressure of O_2 was reduced by half, as previously described (58). Mice were then used for either pulsatile pressure-flow studies (CTL: $n = 6$, HPH: $n = 5$) or microcomputed tomography imaging studies (CTL: $n = 8$, HPH, $n = 5$). For the former, mice were anesthetized with an intraperitoneal injection of 150 mg/kg body wt pentobarbital sodium which has been shown not to affect pulmonary hemodynamics (2, 29, 33). For the latter, mice were anesthetized with 52 mg/kg body wt pentobarbital sodium and then euthanized by exsanguination. In both cases, while the heart was still beating, heparin sodium (200 IU in 0.2 ml) was injected into the RV to prevent blood clotting in the lungs. All protocols and procedures were approved by the University of Wisconsin and Zablocki VA Medical Center Institutional Animal Care and Use Committees.

Pulsatile pressure-flow studies. The isolated, ventilated, perfused mouse lung preparation was used for pulsatile pressure-flow studies as previously developed and validated (58, 59) (Fig. 1). In brief, following euthanasia, the trachea, pulmonary artery, and left atrium were cannulated for ventilation, perfusate inflow, and perfusate outflow, respectively. The tracheal cannula was inserted approximately halfway into the trachea. The pulmonary artery cannula was positioned in main pulmonary artery with the tip just proximal to the first bifurcation. The left atrial cannula was inserted through the mitral valve and then withdrawn until the flares of the tip base abutted the valve annulus. The lungs were ventilated with room air and perfused with heated RPMI 1640 cell culture medium with 3.5% Ficoll (an oncotic agent). A syringe pump (Cole-Parmer, Vernon Hills, IL) was used to create steady pulmonary vascular flow of perfusate, and a high-frequency oscillatory pump (Bose-Electro Force, Eden Prairie, MN) was used in parallel with the syringe pump to superimpose a oscillatory component on the pulmonary vascular flow. Pressure transducers (P75, Harvard Apparatus, Holliston, MA) measured the instantaneous pulmonary artery pressure (PAP) and left atrial pressure (LAP). Instantaneous flow rate (Q) was measured with an in-line flow meter (Transonic Systems, Ithaca, NY). Pressures and flows were monitored by continuous display on a laptop computer and recorded at 200 Hz.

The pulsatile flow rate measurements were performed according to established methods after initial steady pressure-flow measurements of PAP, LAP, and Q at 1 ml/min (58, 59). In particular, pulsatile pressure-flow data were recorded for flow rates of the form $Q = 3 + 2 \sin(2\pi ft)$ ml/min at frequencies (f) = 1, 2, 5, 10, 15, and 20 Hz. At the higher frequencies (15 and 20 Hz), the imposed waveforms were not ideal (1–5 ml/min); maxima (minima) were less (greater) than desired. Nevertheless, the imposed waveforms were not significantly different between control and hypoxic lungs. Above 20 Hz, which is ~2.5 times the heart rate for mice, ~8 Hz in conscious unrestrained mice (52), the deviation from the desired waveform was too high to provide good signal-to-noise ratios in the resulting pressure data. Between protocols, the lungs were allowed to rest for 1 min with

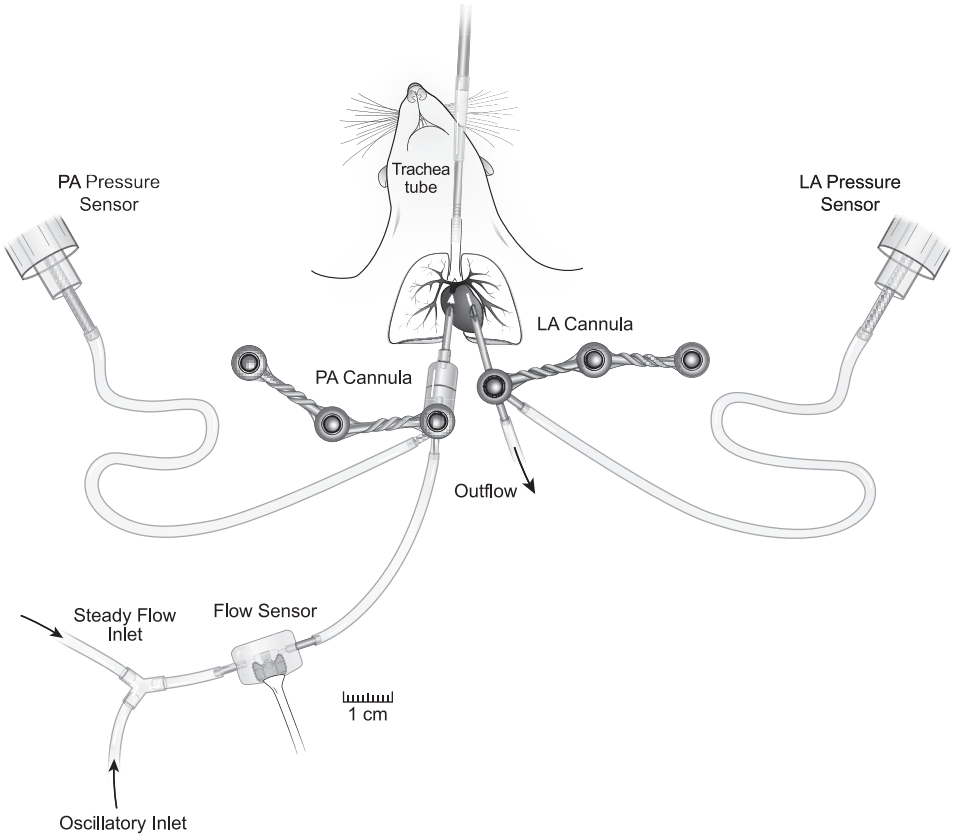

Fig. 1. Schematic of isolated lung setup showing the inlets for steady and oscillatory flow and the sites for measurement of instantaneous pulmonary artery flow rate Q (flow sensor), pulmonary artery pressure (PA pressure sensor), and left atrial pressure (LA pressure sensor).

normal ventilation (2 to 10 cmH_2O at 90 breaths/min) (62) and a steady flow rate of Q = 0.5 ml/min. All data were recorded with the lungs inflated at the end-inspiratory pressure of 10 cmH_2O. In preliminary studies, we observed that lower airway pressures yielded lower PAP values, in a mildly flow-dependent manner. However, we did not observe dramatic differences in this flow dependence between CTL and HPH lungs.

Following measurements in the baseline smooth muscle cell (SMC) tone state, a Rho kinase inhibitor (Y27632; Sigma Chemical, St. Louis, MO) was added to the perfusate to a final concentration of 10^{-5} M to induce a vasodilated state. This concentration was selected on the basis of a literature review of isolated mouse (10) and rat (19, 43) lung studies in which this dose maximally decreased mPAP while still selectively inhibiting Rho kinase (22). Pulsatile pressure-flow measurements were taken 15 min after Y27632 administration, followed by steady flow rate measurements. This time point was chosen to allow the effect of Y27632 to stabilize per prior reports (42, 43).

Calculations for pulsatile pressure-flow studies. Pulmonary vascular impedance magnitude (Z) and phase (Θ) were calculated from one full sinusoidal cycle of $\Delta P = PAP - LAP$ and Q at each frequency tested (f = 1, 2, 5, 10, 15, and 20 Hz). Input impedance Z_0 was calculated by averaging the impedance at the 0th harmonic ($f = 0$ Hz) from all tested frequencies. Characteristic impedance Z_C was calculated as the average of Z values between the first minimum (5 Hz) and the highest frequency imposed (20 Hz) and index of wave reflection R_W was calculated as $(Z_0 - Z_C)/(Z_0 + Z_C)$ (44).

Theoretical Z_C-mPAP and R_W-mPAP relationships. If viscous effects in the artery wall and at the blood-artery interface are neglected, Z_C corresponds to the square root of the inertance divided by the compliance of the proximal segments of the arterial network (38). Alternatively, under similar assumptions, Z_C can be calculated as the product of fluid density and pulse wave velocity divided by the luminal cross-sectional area of the proximal arteries (63). Both approaches reduce to

$$Z_C = \sqrt{\frac{\rho E h}{2\pi^2 r^5}}$$

where E, r, and h are proximal artery elastic modulus, luminal radius, and wall thickness, respectively, and ρ is density of blood.

To predict the dependencies of Z_C and R_W on mPAP, we used a theoretical approach, outlined in the APPENDIX. Essentially, the characteristic impedance depends on E, r, and h where r and h are a function of initial radius and wall thickness (r_0 and h_0, respectively) as well as the mean transmural pressure mPAP. With increasing mPAP, the artery distends such that r increases and h decreases by conservation of mass for a fixed artery length. For a particular set of E, r_0, and h_0 values, Z_C as a function of mPAP can be found exactly (see APPENDIX).

We used an iterative approach to find the combinations of E, r_0, and h_0 that yielded a theoretical Z_C-mPAP relationship that best fit the experimental data. No unique combination of E, r_0, and h_0 was found to minimize error for either the CTL or the HPH data in the baseline SMC tone state or as combined with data in the dilated (with Y27632) state. Therefore, sets of E, r_0, and h_0 values for which the sum of the squared error between experimental and theoretical Z_C was <0.0015 were considered potential solutions. No differences in the potential solution space were found for CTL vs. CTL + Y27632 or for HPH vs. HPH + Y27632. Therefore, extrema of the resulting solution spaces (i.e., parameter sets of E, r_0, and h_0 for best fit to CTL + Y27632 and HPH + Y27632 with maximum and minimum r_0 values) were plotted against experimental data. R^2 values and P values were found for the resulting theoretical Z_C values in relation to the experimental Z_C values. Theoretical R_W values and R_W-mPAP relationships were calculated at these same extrema of the solution space (i.e., parameter sets of E, r_0, and h_0) based on the definition of $R_W = (Z_0 - Z_C)/(Z_0 + Z_C)$, where $Z_0 = Q \times mPAP + LAP$.

Microcomputed tomography imaging studies. Preparation of mouse lungs for microcomputed tomography was modified from methods previously used on rats (25). Briefly, the pulmonary artery and trachea were cannulated (PE-90 tubing, 1.27 mm outer diameter and 0.86 mm inner diameter) and the heart was dissected away. The pulmonary artery cannula was positioned in main pulmonary artery well above the first bifurcation. The lungs were ventilated with 15% O_2-6% CO_2, balance nitrogen, at 90 breaths/min with 4 cmH_2O end-expiratory pressure and 10 cmH_2O end-inspiratory pressure. The lung was rinsed free of blood with a physiological salt solution containing 5% bovine serum albumin, and hemodynamic measurements were taken at flow rates in the range of 0–3 ml/min. The Rho kinase inhibitor Y27632 was administered (10^{-5} M) to dilate the pulmonary vasculature before imaging. The perfusate with Y27632 was allowed to recirculate for 5 min before steady flow rate measurements were retaken.

Following steady flow rate measurements, the cannulas were clamped at end-inspiration and the isolated lungs were placed in the imaging chamber as previously described (25). The lungs were ventilated with the same gas mixture; the perfusate was replaced with perfluorooctyl bromide (PFOB). This vascular contrast agent was selected because perfluorochemicals, which are a good alternative to traditional artificial blood substitutes (20), have been shown to inhibit vasoactivity (49). The lungs were conditioned by cycling the intravascular pressure from 0 to 25 mmHg briefly several times. Then, the arterial pressure was set to 7.4 mmHg, and the lungs were rotated in the X-ray beam at 1° increments to obtain 360 planar images. The pressure was lowered to 6.3 mmHg and then raised to 13.0 and 17.2 mmHg with complete computed tomography scans at each pressure as previously described (24).

Briefly, the microfocal X-ray computed tomography system is composed of a Fein-Focus-100.50 X-ray source (3-μm focal spot) and a North American Imaging AI-5830-HP image intensifier coupled to a Silicon Mountain Design charge-coupled device (CCD) camera. To minimize noise as well as maximize vascular contrast, each planar projection image is a result of averaging seven frames. The image data are transmitted from the CCD camera to a computer. Image acquisition, positional information recording, and stage control are all preformed by in-house, custom-written, Windows-based software running on the workstation. Between each scan, the intravascular pressure was briefly raised to ~25 mmHg and then lowered to each value set for image acquisition. While we attempted to keep the geometry similar from scan to scan, it varied slightly depending on lung size, mostly height. The spatial resolution of a typical volumetric mouse lung scan was between 30 and 40 μm. High-resolution planar images were also captured at each of the four pressures in a randomly selected section in the peripheral parenchyma of each lung. The resolution of these images was in the range of 6 to 8 μm.

The order of pressures was determined from preliminary studies to minimize vascular leakage at higher pressures. Intravascular pressures were maintained hydrostatically and calculated as the difference between the level of PFOB in the reservoir and the center of the lung, taking into account the density of the PFOB. With this technique, only the contrast-filled luminal volumes are detectable, not the walls themselves. As a consequence, direct measurements of wall thickness throughout the lung and as a function of pressure were not possible. After each mouse lung was imaged at all four pressures, a flood field image (lung removed from the beam) and a BB field image (a phantom of a uniform grid of 1-mm diameter stainless steel spheres spaced at 1.5-cm intervals) were taken to be used in the correction for spatial variations and correction for spatial distortion, image intensifier gain, and beam geometry.

Measurements from microcomputed tomography imaging studies. Images of the contrast-filled luminal volumes were preprocessed to correct image intensifier spatial distortion and nonuniform illumination intensity. The 360 planar images were then reconstructed into an isometric three-dimensional (3-D) volume using a Feldkamp cone-beam algorithm.

The reconstructed images were converted to Dicom 3.0 (497 × 497 × 497 pixels) and then imported into the commercially available software package Mimics (Materialise, Leuven, Belgium). Following segmentation, a 3D surface mask of the whole arterial tree was generated (Fig. 2*A*). The right principal pathway was then isolated using 3-D editing by following the path of the largest diameter branch at each bifurcation (Fig. 2*B*). Using the medCAD package in Mimics, which has previously been used to quantify the anatomy and branching morphometry of the abdominal aorta (7, 45), the centerline coordinates and best fit arterial luminal diameter for sections perpendicular to the centerline were generated at a point spacing of 1 pixel along the pathway. The centerline coordinates and corresponding luminal diameters were imported into Matlab (MathWorks, Natick, MA) for postprocessing data reduction. Each segment of the principal pathway was characterized by a distance from the origin (located at the end of the cannula) and a diameter, and dimensions were converted using the luminal diameter of the cannula for calibration (Fig. 2*C*). The length of each segment was calculated as the distance between the postbifurcation points. Measurements were made on arteries ranging in size from 1,200 to ~80 μm in diameter. On the basis of an assumed error in the centerline coordinates and diameter fits from Mimics of 1 pixel, the average percent error in the length measurement was found to be approximately 2.5% and 12% for the longest and shortest vessels, respectively; error in the diameter measurement was about 4% and 18% for the largest and smallest vessels, respectively. The absolute measurement errors were less than the standard deviations of the diameter and length in CTL and HPH groups.

Calculations for microcomputed tomography imaging studies. The distensibilities of the intralobar and extralobar arteries were calculated from multiple measurements made in the same lung at different intravascular pressures at identical locations in the principal pathway (Fig. 2*C*). The pressure in individual segments was calculated on the basis of the height difference with respect to the center of the lung (the hydrostatic gradient reference point). A morphometric model (39) was applied to the arterial diameters as a function of distance from the main trunk inlet (x) and pressure (P) to calculate distensibility of the principal pathway (α_{lung}) from the following equation: $D_{(x,P)} = D_{(0,0)}(1 + \alpha_{lung} P)(1 - x/L_{tot})^c$, where $D_{(0,0)}$ is the unstressed diameter of the main pulmonary artery ($x = 0$), L_{tot} is the total length of the principal pathway, and c is a measure of the taper of the principal pathway. Using the relationship between the cumulative number of branches (N_{BR}) and the distance along the main trunk (L_{tot}), an estimate of the total number of branches off the main trunk (N_{tot}) was calculated from: $N_{BR}(x) = N_{tot}[1 - (1 - x/L_{tot})]^b$, where b is a measure of the branch distribution along the principal pathway. For the extralobar right pulmonary artery (RPA), we quantified distensibility (α_{RPA}) using the linear pressure vs. diameter relationship proposed by Yen et al. (64) and used by Molten et al. (39): $\alpha_{RPA} = \beta/D_{(x,0)}$, where $\beta = (D_{(x,P)} - D_{(x,0)})/P$. Compliance of the RPA (C_{RPA}) was calculated as α_{RPA} times the luminal cross-sectional area of the unstressed RPA (63).

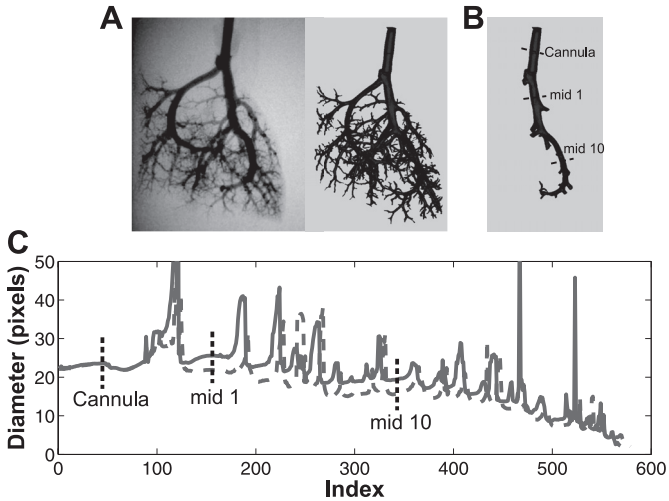

Fig. 2. *A*: planar images were reconstructed into three-dimensional (3-D) volumes and imported into Mimics. *B*: a 3-D surface mask was generated from which the right principal pathway was isolated. Using the medCAD package in Mimics, the centerline coordinates and best fit diameters were found for the principal pathway. *C*: from all of the diameter measurements, the data were reduced to the diameter of each branch by finding the midsegment diameter. Representative measurements are shown of the midbranch diameter for the first segment (*mid 1*) and the 10th segment (*mid 10*) as well as the pulmonary artery cannula (Cannula) at a lower pressure (dashed gray line) and a higher pressure (solid gray line).

Structural changes in the distal vasculature (arteries with diameters <150 μm) were quantified from high-magnification planar images of mouse pulmonary arteries. The diameter of each artery in a 2 × 2 mm square containing one terminal branch was measured by an observer blinded to experimental conditions. Lungs for which images had overlapping terminal branches or incomplete branches were excluded. In each lung the frequency of arteries in the size ranges 20–50 μm, 50–100 μm, and 100–150 μm were counted at each pressure.

Statistical analysis. Absolute changes in study endpoints with regard to state (baseline SMC tone vs. dilated with Y27632) and exposure (CTL vs. HPH) were analyzed using a generalized least squares (GLS) for repeated measures with an unstructured variance-covariance structure. The three-way comparison of factors (state, exposure, and frequency) was significant, which led to the construction of contrast matrices to investigate changes in Z due to state and exposure as a function of frequency. GLS models with two-way comparisons (state and exposure) were constructed to analyze changes in study endpoints mPAP, Z_0, Z_C, and R_W. If there was a significant interaction of factors, contrast matrices were constructed to investigate changes in endpoints as a function of state.

To investigate changes in the frequency of distal arteries, a GLS model with two-way comparison of factors (exposure and pressure) was used. Structural data endpoints (L_{tot}, N_{BR}, α_{lung}, $D_{(0,0)}$, α_{RPA}, C_{RPA}, RPA length) were analyzed by one-way analysis of variance to analyze differences between control and hypoxic lungs. No violations of the normality assumption were found, and $P < 0.05$ was considered significant. All P values were two-sided, and all statistical analyses were performed using R software (http://www.R-project.org/, version 2.5.1). All data are presented in terms of means ± SD.

RESULTS

In both control and hypoxic lungs, Y27632 decreased PAP (Fig. 3). In the Y27632 state with a steady flow of 3 ml/min, chronic hypoxic lungs continued to have elevated pressures when compared with control lungs. This persistent effect of chronic hypoxia in the presence of acute Rho kinase inhibition was investigated using high-magnification images of the terminal branches. Qualitatively, fewer small arteries were detectable in HPH lungs compared with CTL lungs (Fig. 4, *B* vs. *A*). Quantitatively, hypoxic and control lungs had the same number of measured arteries 100–150 μm; however, hypoxia caused functional rarefaction of the arteries 50–100 μm in diameter even with acute Rho kinase inhibition (Fig. 4*C*). Also, there was a significant increase in number of arteries 50–100 μm in diameter measured at 17 mmHg in the CTL lungs but there was no change in HPH lungs. The frequency of the smallest visible arteries, 20–50 μm, tended to decrease with increased vascular pressure, but the change was not significant.

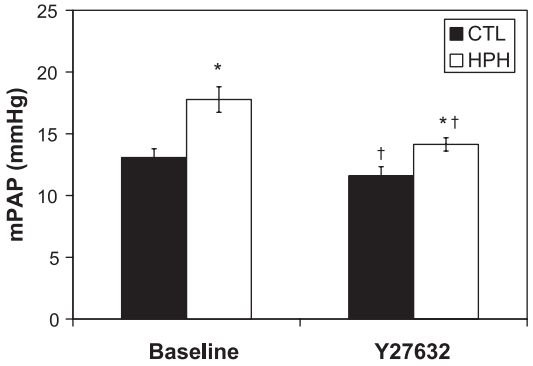

Fig. 3. Mean pulmonary arterial pressure (mPAP) at 3 ml/min for control (CTL; $n = 6$) and hypoxic pulmonary hypertension (HPH; $n = 5$) mouse lungs in the baseline smooth muscle cell (SMC) tone state and with Y27632. *$P <$ 0.05 vs. 0-day; †$P < 0.05$ Y27632 vs. baseline.

To determine the ability of acute Rho kinase inhibition to reduce or eliminate chronic hypoxia-induced changes in RV afterload, pulsatile pressure-flow relationships in CTL and HPH lungs with and without perfusion with Y27632 were analyzed. All impedance spectra had the expected "L"-shape with a high amplitude at zero frequency and a rapid decline to low amplitudes at higher frequencies with moderate oscillations; the phase angles were negative at low frequencies and approached zero at higher frequencies (Fig. 5). In control lungs (Fig. 5*A*), Y27632 decreased Z_0 and shifted the ratio of pressure to flow moduli to higher pressures at high frequencies. As a consequence, Y27632 tended to increase Z_C; the increase in Z_C combined with the decreased Z_0 led to a decrease in R_w (Table 1). Phase angle was unaffected. In hypoxic lungs (Fig. 5*B*), Y27632 decreased Z_0 and had no effect on the ratio of pressure to flow moduli at high frequencies, resulting in no change of Z_C. Here, the decrease in Z_0 relative to Z_C resulted in a decrease in R_W.

Either with or without Rho kinase inhibition, chronic hypoxia increased Z_0 and decreased the magnitude at higher frequencies, resulting in a crossover between the two PVZ spectra. Hypoxia tended to affect phase angle, but no significant effect as a function of frequency was found (Fig. 5*C*; with Y27632 shown only).

The contribution of proximal arterial size and compliance to pulsatile pressure-flow measurements in the isolated lungs was investigated using the theoretical relationships between the impedance metrics Z_C and R_W and mPAP. Theoretical Z_C was calculated for proximal artery elastic modulus, E, from 60 to 250 kPa; wall thickness, h_0, from 60 to 250 μm; and luminal diameter, $D_0 = 2r_0$ from 800 to 2,000 μm. The combinations of E, h_0, and D_0 that were considered solution spaces had a total squared sum of error <0.0015. In CTL lungs, the baseline and Y27632 states were well described by a proximal artery elastic modulus E in the range of 100 to 240 kPa, wall thickness h between 25 and 50 μm, and inner diameter of 1,010 to 1,160 μm (Fig. 6 solid lines: bounding fits; $R^2 = 0.51$; $P <$ 0.01). The HPH lungs could be described by $E = 235$–250 kPa, $h = 120$–200 μm, and inner diameter = 1,690–1,940 μm (Fig. 6, dashed lines: bounding fits; R^2=0.057; $P = 0.5$).

Like Z_C, R_W exhibited a marked dependency on mean PAP (Fig. 7). For the solution spaces for a good fit of theoretical Z_C-mPAP relationship to experimental data in CTL and HPH lungs given above, R_W as a function of mPAP was calculated. The resulting curvilinear relationships fit the experimental results for CTL and HPH conditions well (CTL: $R^2 = 0.97$; $P < 0.001$, HPH: $R^2 = 0.99$; $P < 0.001$).

Despite these significant differences in PVZ metrics between CTL + Y27632 and HPH + Y27632, few differences were evident in the imaging analysis of whole mouse lungs. In particular, total length (L_{tot}), number of branches, α_{RPA}

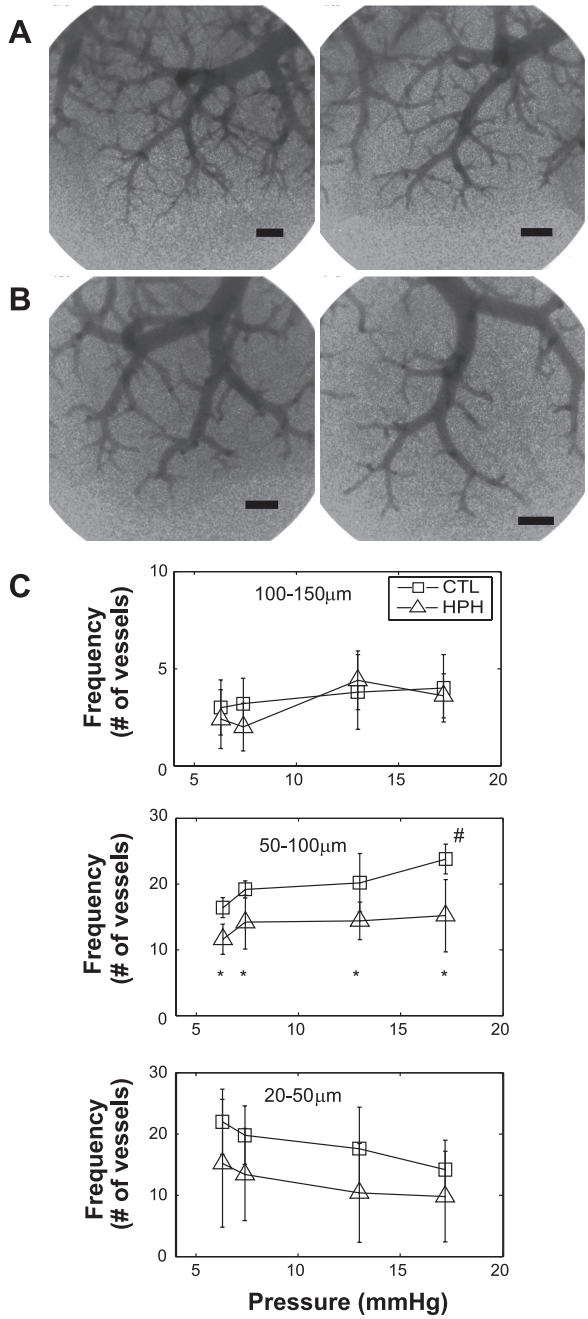

Fig. 4. *A* and *B*: high-magnification planar images of terminal branches of pulmonary arteries in CTL ($n = 5$; *A*) and HPH ($n = 5$; *B*) mouse lungs. Bar length is 500 μm. *C*: frequency of arteries, 20–50, 50–100, and 100–150 μm in diameter, in CTL and HPH lungs as a function of pressure. All lungs were perfused with Y27632 before imaging. Qualitatively and quantitatively, the HPH lungs have fewer visible distal branches than CTL lungs. *$P <$ 0.05 vs. CTL. #$P < 0.05$ vs. 6.3 mmHg.

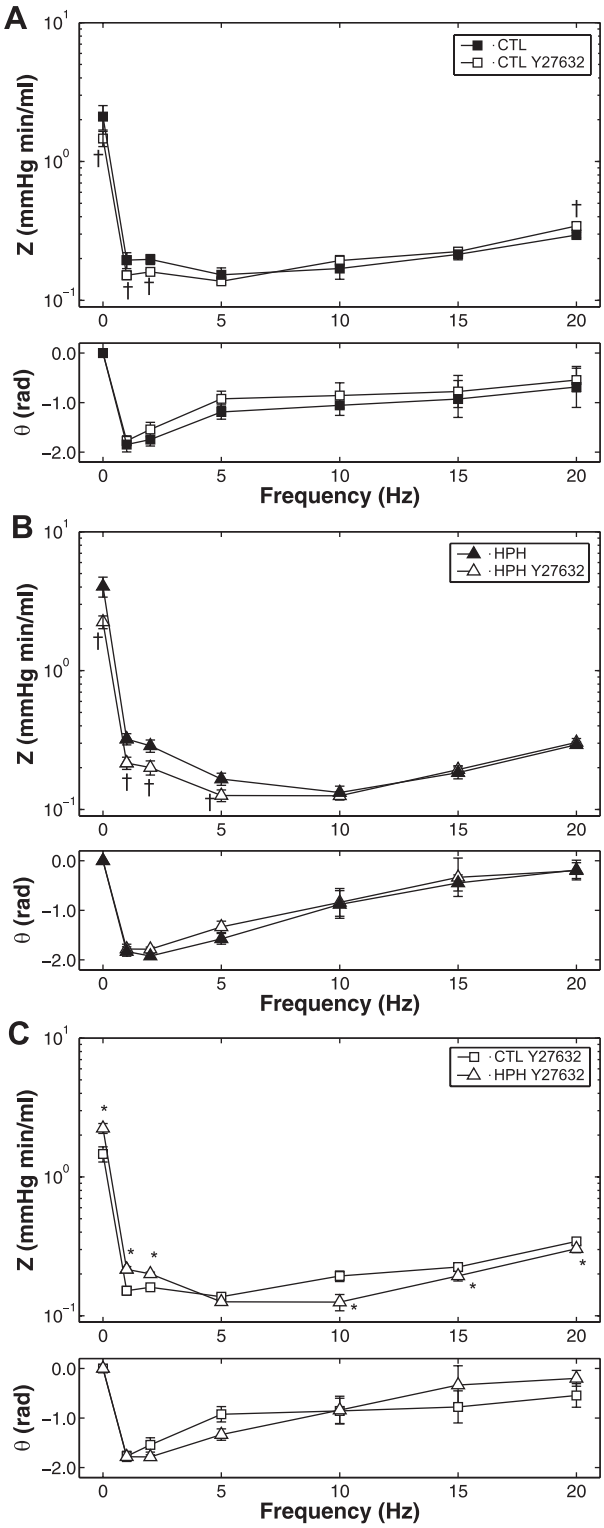

Fig. 5. Pulmonary vascular impedance magnitude (Z) and phase (θ) spectra in isolated perfused lungs from CTL ($n = 6$; *A*) and HPH ($n = 5$; *B*) mouse lungs in a baseline SMC tone state and with Y27632 and from CTL and HPH mouse lungs with Y27632 (*C*). *$P < 0.05$ vs. 0-day; †$P < 0.05$, for change from baseline to Y27632.

and α_{lung} and length were not different (Table 2). Only the extrapolated zero pressure diameter of the main pulmonary artery ($D_{(0,0)}$) and C_{RPA} were significantly affected by HPH after acute Rho kinase inhibition (Table 2; both $P < 0.05$).

DISCUSSION

The main findings of the present study are that acute Rho kinase inhibition nearly normalizes increases in mPAP and pulmonary vascular resistance caused by chronic hypoxia but that proximal arterial thickening and stiffening persist. Stiffening was evident in proximal arteries from imaging studies at controlled pressures (C_{RPA}) as well as from pulsatile pressure-flow relationships (Z_C-mPAP relationship); thickening was evident from the analysis of pressure-flow relationships. Interestingly, despite the nearly normalized mPAP and Z_0, acute Rho kinase inhibition did not eliminate chronic hypoxia-induced apparent pruning of small pulmonary arteries 50 to 100 μm in diameter. This finding refutes the hypothesis proposed by some (55) that apparent pruning is due to persistent pulmonary vasoconstriction and not structural remodeling.

Recent studies in mice and rats have found that persistent vasoconstriction mediated by Rho kinase activation is a major contributor to increased pulmonary vascular resistance caused by HPH (10, 19, 35, 43). In vivo, chronic administration of Y27632 decreased RV systolic pressure by 10% in the lungs of mice exposed to HPH (10) and acute administration of Y27632 decreased RV peak systolic pressures in the lungs of rats exposed to HPH by 35% (19) and 20% (43). Similar decreases were found ex vivo in isolated rat lungs; administration of 10^{-6} M Y27632 decreased PAP by 15% (19, 43). A 10-times higher concentration decreased PAP by 30% in HPH lungs and 20% in CTL lungs of rats (43). In our isolated mouse lungs, the effect of Y27632 at 3 ml/min was less; a concentration of 10^{-5} M Y27632 decreased PAP by 20% in HPH lungs and 10% in CTL lungs. At a typical isolated perfused lung flow rate of 1 ml/min, it was comparable; Y27632 decreased PAP by 30% in HPH lungs and 20% in CTL lungs. Thus, our results confirm that the predominant mechanism of increased pulmonary vascular resistance with exposure to hypoxia on the order of weeks is persistent pulmonary vasoconstriction in resistance arteries; i.e., reactive changes in distal arteries.

The mechanisms of changes in conduit arteries appear different. In large arteries, we and others have found that reactive changes are minimal, whereas fixed changes are significant. That is, previous direct measurements of arterial deformation with increasing pressure have demonstrated that HPH decreases the compliance of extralobar pulmonary arteries in passive and Rho kinase-inhibited states (27, 56); i.e., HPH causes proximal artery stiffening as found here (C_{RPA}; Table 2). Our impedance-derived estimates of proximal segment elastic modulus and wall thickness changes with HPH support fixed changes in proximal arteries that lead to increased stiffness. We have postulated that increased arterial wall strain due to hypertension stimulates smooth muscle cells to increase collagen production as a way of normalizing circumferential stress and strain (27, 56); others have suggested that the adventitial fibroblast response to hypoxia via p38 mitogen-activated protein kinase (1, 40), transcription of hypoxia-inducible factor-1α (54), and the expression of early growth response-1 (15) is responsible for increased collagen and other extracellular matrix components (12, 47). We note, however, that species-dependent differences have been identified in mechanisms of HPH-induced proximal artery remodeling. In particular, adventitial cells appear to play a larger role in large

Table 1. *Metrics of impedance (Z_0, Z_C, R_W) for CTL ($n = 6$) and HPH ($n = 5$) mouse lungs in the baseline SMC tone state and with Y27632*

	Z_0, mmHg·min·ml^{-1}		Z_C, mmHg·min·ml^{-1}		R_W (dimensionless)	
	CTL	HPH	CTL	HPH	CTL	HPH
Baseline	2.1 ± 0.4	4.0 ± 0.7*	0.21 ± 0.01	0.194 ± 0.009	0.81 ± 0.05	0.91 ± 0.01*
Y27632	1.5 ± 0.2†	2.2 ± 0.2*†	0.22 ± 0.01	0.187 ± 0.005*	0.73 ± 0.03†	0.84 ± 0.02*†

Values are means ± SD. Z_0, 0-Hz impedance; Z_C, characteristic impedance; R_W, wave reflection; CTL, control; HPH, hypoxic pulmonary hypertension; SMC, smooth muscle cell. *$P < 0.05$ vs. CTL; †$P < 0.05$, for change from baseline to Y27632.

animals whereas medial cells play a larger role in smaller animals, including rodents (53).

Some fixed changes in resistance arteries were found here, via microcomputed tomography imaging and Rho kinase inhibition-resistant increases in mPAP and Z_0. We interpret the imaging results as "apparent pruning" because we speculate that there is not an actual loss of small arteries as previously suggested (17, 36, 37, 48), but instead a functional narrowing that prohibits PFOB contrast infusion and thus optical detection. The frequency of vessels 20–50 μm tended to decrease with increased pressure, suggesting that as pressure increased, the vessels distended, resulting in an increase in frequency of vessels 50–100 μm. Confirmation of this suggestion must await development of higher-resolution imaging modalities or different contrast agents that allow detection of artery diameters continuously from 50–100 μm in diameter down to the capillary level. Previously, we have demonstrated increased collagen-related gene expression in lung tissue of mice exposed to hypoxia (9); even in these small resistance arteries we postulate that increased arterial wall strain stimulates smooth muscle cells to increase collagen production to normalize circumferential stress and strain.

We calculated whole lung distensibility, α_{lung} to further assess fixed changes in the lung vasculature, but this did not decrease with HPH (Table 2). The sensitivity of this parameter to HPH-induced pulmonary vascular remodeling is unclear. While it incorporates proximal and distal arterial mechanics, it is more sensitive to distal arterial mechanics than proximal arterial mechanics (31). The lack of significant changes in α_{lung} may be due to the relatively short duration of hypoxia (10 days). We predict that as duration of chronic hypoxia increases, the proportion of fixed to reactive changes in the lung increases, at least up to some point of stabilization. Prior work from our group has found no significant differences in proximal arterial mechanics, pulmonary vascular resistance or pulmonary vascular impedance between 10 and 15 days of hypoxia exposure (27, 58), but those studies did not explore fixed vs. reactive changes. As shown here, 10 days of hypoxia was sufficient to induce significant reactive and some fixed changes in distal arteries and fixed but not reactive changes in the proximal arteries. The latter finding is supported by our recent work on the effects of vasoactivity and HPH on extralobar pulmonary artery biomechanics (56).

Our results are inconsistent on the effect of HPH on extralobar artery size. Direct measurements of RPA diameter show no change with HPH, but the whole lung pulmonary arterial luminal surface fitting approach to find $D_{(0,0)}$ demonstrates a decrease (Table 2). Direct measurements in isolated extralobar arteries have shown that HPH does not alter diameter at low pressures (27, 56). Moreover, the impedance-derived proximal segment diameter estimates suggest that HPH increases proximal artery diameter. We speculate that the whole lung morphometry surface fitting underestimates $D_{(0,0)}$ in HPH lungs because of sensitivity to the distal arteries and that, in fact, no

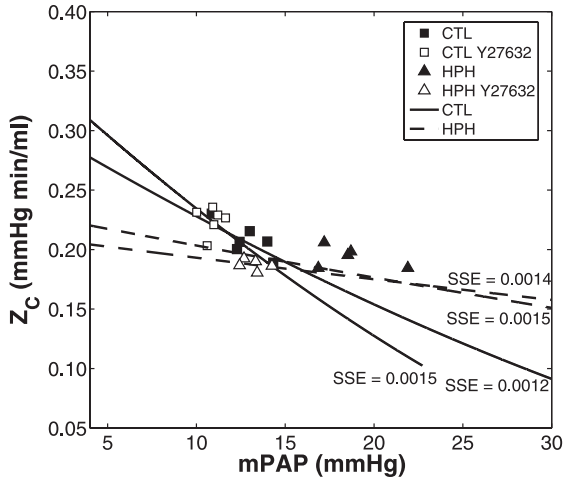

Fig. 6. Characteristic impedance (Z_C) as a function of mPAP for CTL ($n = 6$; □ and ■) and HPH ($n = 5$; ▲ and △) mouse lungs in a baseline SMC tone state and with Y27632 (white). The extrema of the solution spaces for the theoretical Z_C-mPAP relationships are shown by the bounding areas for CTL (solid lines) and HPH (dashed lines). Sum of squared error (SSE) for each model fit to experimental data is shown.

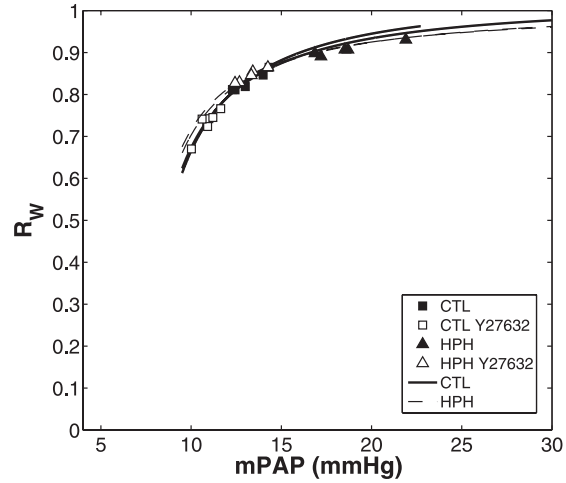

Fig. 7. Index of wave reflection (R_W) as a function of mPAP for CTL ($n = 6$; □ and ■) and HPH ($n = 5$; ▲ and △) mouse lungs in a baseline SMC tone state and with Y27632 (white). Overall, Y27632 decreased mPAP but did not shift the R_W-mPAP relationship. The extrema of the solution spaces for the theoretical R_W-mPAP relationship are shown by the bounding areas for CTL (solid lines) and HPH (dashed lines).

Table 2. *Structural parameters of the mouse pulmonary vasculature measured from micro-CT images of isolated mouse lungs with Y27632*

Parameter	CTL	HPH	*P* Value
L_{tot}, mm	18.7 ± 0.9	18.0 ± 0.7	0.14
N_{BR}	28 ± 4	25 ± 5	0.19
α_{lung}, %/mmHg	2.3 ± 0.8	2.7 ± 1.0	0.52
$D_{(0,0)}$, μm	760 ± 60	650 ± 80*	0.02
α_{RPA}, %/mmHg	2.5 ± 1.1	1.9 ± 0.6	0.26
C_{RPA}, mm^2/mmHg	0.011 ± 0.004	0.006 ± 0.002*	0.04
RPA length, mm	2.9 ± 0.3	3.1 ± 0.3	0.27
RPA diameter, μm	740 ± 60	740 ± 50	0.93

Values are means ± SD. CT, computed tomography; L_{tot}, total length; N_{BR}, number of branches; α_{lung}, whole lung distensibility; $D_{(0,0)}$, unstressed diameter of main pulmonary artery; α_{RPA}, right pulmonary artery distensibility; C_{RPA}, RPA compliance. *$P < 0.05$ vs. CTL.

change occurs. Also, the impedance-derived proximal artery diameter estimates are for an idealized "effectively proximal" artery that includes extralobar and intralobar arteries, and may include some intermediate arteries. This is consistent with findings in rats where the first generation branch was found to be larger in chronically hypoxic lungs than control lungs (51). The impedance-derived proximal artery wall thickening finding cannot be confirmed by microcomputed tomography since only the contrast-filled regions are visible, but it is supported by prior isolated vessel experiments (27, 56). Interestingly, the overall findings of the impedance-derived structural analysis—that HPH increases proximal artery elastic modulus, wall thickness, and luminal diameter—are supported by prior studies (27, 56) despite a poor fit of the theoretical model to the experimental data in this condition ($R^2 = 0.057$; Fig. 6). The increase in R_W with HPH, which could cause wave reflections to return earlier, may weaken the assumption that the high-frequency components of PVZ are reflection free. Alternatively, HPH may be associated with changes in the proximal arteries not captured in the simple model we propose here. Further work is needed to develop a more sophisticated model of proximal arterial mechanics that would provide additional, useful insights into pulmonary hemodynamics and changes with HPH.

We have previously shown that HPH decreases characteristic impedance and increases wave reflections (58) and that the Z_C-mPAP relationship provides insight into the effects of vasoactive agents and hypoxia on the proximal and distal vasculature (60). Here we show that acute Rho kinase inhibition does not eliminate these effects of HPH on RV afterload; the same functional differences in pulsatile pressure-flow relationships persist with acute Rho kinase inhibition. In addition, we were able to demonstrate structural changes induced by chronic hypoxia that account for these functional changes. In particular, we found decreased compliance (i.e., stiffening) of the right main extralobar artery by microcomputed tomography with few other changes to whole lung morphometry, findings that are supported by our theoretical analysis of Z_C-mPAP and R_W-mPAP relationships and prior work as noted above. That is, because of the pressure-dependency of Z_C, both Z_C and compliance decrease with HPH.

Our experimental approach enables us to differentiate between reactive (Rho kinase-dependent) and fixed (Rho kinase-independent) changes induced by chronic hypoxia. While the approach is robust, these results may be dependent on the species we chose, the duration of hypoxia, and even the strain of mouse. Indeed, significant strain-dependent differences have been found in mouse lungs in response to chronic hypoxia (57), which may complicate comparisons to transgenic and knockout strains on a non-C57BL6 background. In C57BL6 male mice after 10 days of chronic hypoxia, we found evidence of fixed changes in the proximal vasculature and both reactive and fixed changes in the distal vasculature. The fixed structural changes in the proximal vasculature include stiffening of the proximal, conduit arteries, which is consistent with previous clinical (4, 23, 50) and experimental studies (8, 26–28, 54). Evidence of reactive changes in the distal arteries includes the significant drop in PAP and Z_0 with administration of Y27632, which is supported by prior literature as noted above (10, 19, 43); evidence of fixed changes include the apparent loss of small arteries in a Rho kinase-inhibited state (Fig. 4) and the persistent difference in Z_0 between CTL and HPH lungs in the Rho kinase-inhibited state.

Limitations. We did not obtain PVZ results above 20 Hz, which is only twice the native heart rate of the mouse (52), because the system cannot generate higher-frequency oscillations in flow sufficiently close to the desired magnitude (1 to 5 ml/min). We cannot exclude that additional information could be obtained at higher frequencies and that our calculation of Z_C would change if these were included. However, in vivo the lower harmonics contain the most power and thus the most information (38). In addition, our calculations of impedance spectra are based on pulsatile waveforms with single frequencies that were imposed in a fixed order. Time-dependent effects, such as loss of drug efficacy or increased pulmonary vascular permeability, could therefore have affected our higher-frequency data more than our lower-frequency data. However, given the short duration of all pulsatile flow trials (66 s in total for three sequential trials from $f = 1$ to 20 Hz), this effect is likely to be small.

In the isolated perfused lung system, because of the lower than physiological flow rate (by about 3-fold) and perfusate viscosity (by 3- to 4-fold), mean PAP is lower than commonly reported in vivo in control and hypoxic mice (10). Since, as we show here, Z_C and R_W are highly pressure dependent, this difference likely affects the measured values of impedance metrics. Our use of a fixed airway pressure, at end-inspiration, while pressure-flow measurements are obtained is also different from the in vivo condition. Thus, at this time, our results cannot be compared with in vivo measurements of impedance.

Conclusion. Our results demonstrate that acute administration of Y27632 has dramatic effects on small resistance arteries in the pulmonary circulation. Our results also show that Y27632 has little or no direct effect on the large conduit arteries that significantly impact RV afterload. These findings support the idea that fasudil decreases resistance of small arteries with no change in the compliance of the large arteries, which may explain its lack of efficacy for treatment of severe pulmonary hypertension.

APPENDIX

In an artery with intramural pressure P and zero extramural pressure, the circumferential stress at a radial distance r is given by

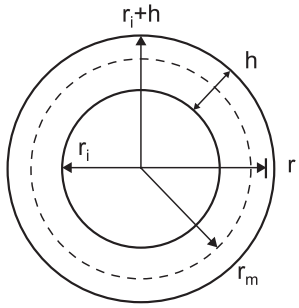

Fig. A1. Definitions of radial distance (r), inner radius (r_i), wall thickness (h), outer radius ($r_i + h$), and midwall radius (r_m) that are used to derive theoretical Z_C-mPAP relationship.

$$\sigma(r) = P\frac{r_i^2\left[r^2 + (r_i + h)^2\right]}{r^2\left[(r_i + h)^2 - r_i^2\right]} \tag{A1}$$

(16) where r_i is the inner radius and h is the wall thickness such that $r_i \le r \le r_i + h$ (Fig. A1). The stress at the midwall radius r_m is then

$$\sigma_m = P\frac{r_i^2\left[r_m^2 + (r_i + h)^2\right]}{r_m^2\left[(r_i + h)^2 - r_i^2\right]} \tag{A2}$$

We introduce the midwall radius here because if we compute the midwall stress and strain referenced to the no-load midwall radius, we can reasonably ignore the effects of residual stresses (65). The midwall strain (ε_m) referenced to the no-load midwall radius (r_{m0}) is

$$\varepsilon_m = \frac{1}{2}\left[\left(\frac{r_m}{r_{m0}}\right)^2 - 1\right] \tag{A3}$$

by Green's formulation assuming large deformations ($\varepsilon \sim 1$). Finally, the midwall stress and strain are related by the elastic modulus E assuming a linearly elastic material where

$$\sigma_m = E\varepsilon_m \tag{A4}$$

Substituting *Eqs. A2* and *A3* into *Eq. A4*, we obtain

$$P\frac{r_i^2}{r_m^2}\frac{\left(r_m^2 + (r_i + h)^2\right)}{\left[(r_i + h)^2 - r_i^2\right]} = E\frac{1}{2}\left[\left(\frac{r_m}{r_{m0}}\right)^2 - 1\right] \tag{A5}$$

Exploiting the geometric relationship

$$r_i = r_m - h/2 \tag{A6}$$

we obtain

$$P\frac{(r_m - h/2)^2}{r_m^2}\frac{\left[r_m^2 + (r_m + h/2)^2\right]}{\left[(r_m + h/2)^2 - (r_m - h/2)^2\right]} = E\frac{1}{2}\left[\left(\frac{r_m}{r_{m0}}\right)^2 - 1\right] \tag{A7}$$

which can be rewritten to yield

$$\frac{2r_m^4 - hr_m^3 - \frac{1}{4}h^2r_m^2 + \frac{1}{16}h^4}{2hr_m^3} = \frac{E}{2P}\left[\left(\frac{r_m}{r_{m0}}\right)^2 - 1\right] \tag{A8}$$

Equation A8 can then be rearranged into a polynomial expression in r_m

$$\left(2 - \frac{E}{P}\frac{hr_m}{r_{m0}^2}\right)r_m^4 + \left(\frac{E}{P} - 1\right)hr_m^3 - \frac{1}{4}h^2r_m^2 + \frac{1}{16}h^4 = 0 \tag{A9}$$

However, this equation implicitly depends on P, because h is a function of P, so we invoke conservation of mass for the artery from the no-load state to the deformed state with no change in length as

$$\pi(r_m + h/2)^2 - \pi(r_m - h/2)^2 = \pi(r_{m0} + h_0/2)^2 - \pi(r_{m0} - h_0/2)^2 \tag{A10}$$

where h_0 is the no-load wall thickness. This relationship can be more simply expressed

$$hr_m = h_0r_{m0} \tag{A11}$$

such that *Eq. A9* can be rewritten with only explicit dependence on P

$$\left(2 - \frac{E}{P}\frac{h_0}{r_{m0}}\right)r_m^4 + \left(\frac{E}{P} - 1\right)(h_0r_{m0})r_m^2 - \frac{1}{4}(h_0r_{m0})^2 + \frac{1}{16}\left(\frac{h_0r_{m0}}{r_m}\right)^4 = 0 \tag{A12}$$

Or, more simply

$$\left(2 - \frac{E}{P}\frac{h_0}{r_{m0}}\right)r_m^8 + \left(\frac{E}{P} - 1\right)(h_0r_{m0})r_m^6 - \frac{1}{4}(h_0r_{m0})^2r_m^4 + \frac{1}{16}(h_0r_{m0})^4 = 0 \tag{A13}$$

This polynomial expression can be solved explicitly for r_m in terms of E, r_{m0}, h_0, and pressure P. Then, given r_m, we can solve for h and derive

$$Z_C = \sqrt{\frac{\rho Eh}{2\pi^2(r_m - h/2)^5}} \tag{A14}$$

ACKNOWLEDGMENTS

The authors thank Jens Eickhoff and Victoria Rajamanickam for guidance on the statistical analyses.

GRANTS

This research was supported by the Belgium-Luxembourg Fulbright Scholar Program (to N. C. Chesler) and by National Institutes of Health Grants 1R01HL086939 (to N. C. Chesler) and 1UL1RR025011 (from the Clinical and Translational Science Awards program of the National Center for Research Resources, National Institutes of Health).

DISCLOSURES

No conflicts of interest, financial or otherwise, are declared by the author(s).

REFERENCES

1. **Belknap J, Orton E, Ensley B, Tucker A, Stenmark K.** Hypoxia increases bromodeoxyuridine labeling indices in bovine neonatal pulmonary arteries. *Am J Respir Cell Mol Biol* 16: 366–371, 1997.
2. **Benumof J.** One-lung ventilation and hypoxic pulmonary vasoconstriction: implications for anesthetic management. *Anesth Analg* 64: 821–833, 1985.
3. **Bogaard H, Natarajan R, Henderson S, Long C, Kraskauskas D, Smithson L, Ockaili R, McCord J, Voelkel N.** Chronic pulmonary artery pressure elevation is insufficient to explain right heart failure. *Circulation* 120: 1951–1960, 2009.
4. **Bogren H, Klipstein R, Mohiaddin R, Firmin D, Underwood S, Rees R, Longmore D.** Pulmonary artery distensibility and blood flow patterns: a magnetic resonance study of normal subjects and of patients with pulmonary arterial hypertension. *Am Heart J* 118: 990–999, 1989.
5. **Castelain V, Chemla D, Humbert M, Sitbon O, Simonneau G, Lecarpentier Y, Hervé P.** Pulmonary artery pressure-flow relations after prostacyclin in primary pulmonary hypertension. *Am J Respir Crit Care Med* 165: 338–340, 2002.
6. **Champion H, Michelakis E, Hassoun P.** Comprehensive invasive and noninvasive approach to the right ventricle-pulmonary circulation unit: state of the art and clinical and research implications. *Circulation* 120: 992–1007, 2009.
7. **Doyle B, Callanan A, Burke P, Grace P, Walsh M, Vorp D, McGloughlin T.** Vessel asymmetry as an additional diagnostic tool in the

assessment of abdominal aortic aneurysms. *J Vasc Surg* 49: 443–454, 2009.
8. **Drexler ES, Quinn TP, Slifka AJ, McCowan CN, Bischoff JE, Wright JE, Ivy DD, Shandas R.** Comparison of mechanical behavior among the extrapulmonary arteries from rats. *J Biomech* 40: 812–819, 2007.
9. **Estrada K, Chesler N.** Collagen-related gene and protein expression changes in the lung in response to chronic hypoxia. *Biomech Model Mechanobiol* 8: 263–272, 2009.
10. **Fagan K, Oka M, Bauer N, Gebb S, Ivy D, Morris K, McMurtry I.** Attenuation of acute hypoxic pulmonary vasoconstriction and hypoxic pulmonary hypertension in mice by inhibition of Rho-kinase. *Am J Physiol Lung Cell Mol Physiol* 287: L656–L664, 2004.
11. **Fukumoto Y, Matoba T, Ito A, Tanaka H, Kishi T, Hayashidani S, Abe K, Takeshita A, Shimokawa H.** Acute vasodilator effects of a Rho-kinase inhibitor, fasudil, in patients with severe pulmonary hypertension. *Heart* 91: 391–392, 2005.
12. **Gabbiani G.** The myofibroblast in wound healing and fibrocontractive diseases. *J Pathol* 200: 500–503, 2003.
13. **Galiè N, Manes A, Negro L, Palazzini M, Bacchi-Reggiani M, Branzi A.** A meta-analysis of randomized controlled trials in pulmonary arterial hypertension. *Eur Heart J* 30: 394–403, 2009.
14. **Gan C, Lankhaar J, Westerhof N, Marcus J, Becker A, Twisk J, Boonstra A, Postmus P, Vonk-Noordegraaf A.** Noninvasively assessed pulmonary artery stiffness predicts mortality in pulmonary arterial hypertension. *Chest* 132: 1906–1912, 2007.
15. **Gerasimovskaya E, Ahmad S, White C, Jones P, Carpenter T, Stenmark K.** Extracellular ATP is an autocrine/paracrine regulator of hypoxia-induced adventitial fibroblast growth. Signaling through extracellular signal-regulated kinase-1/2 and the Egr-1 transcription factor. *J Biol Chem* 277: 44638–44650, 2002.
16. **Gere JM, Timoshenko SP.** *Mechanics of Materials*. Boston, MA: PWS Pub, 1997, p. xvi, 912 p.
17. **Hislop A, Reid L.** New findings in pulmonary arteries of rats with hypoxia-induced pulmonary hypertension. *Br J Exp Pathol* 57: 542–554, 1976.
18. **Homma N, Nagaoka T, Karoor V, Imamura M, Taraseviciene-Stewart L, Walker L, Fagan K, McMurtry I, Oka M.** Involvement of RhoA/Rho kinase signaling in protection against monocrotaline-induced pulmonary hypertension in pneumonectomized rats by dehydroepiandrosterone. *Am J Physiol Lung Cell Mol Physiol* 295: L71–L78, 2008.
19. **Hyvelin JM, Howell K, Nichol A, Costello CM, Preston RJ, McLoughlin P.** Inhibition of Rho-kinase attenuates hypoxia-induced angiogenesis in the pulmonary circulation. *Circ Res* 97: 185–191, 2005.
20. **Isaka M, Sakuma I, Imamura M, Makino Y, Fukushima S, Nakai K, Shiiya N, Kenmotsu O, Kitabatake A, Yasuda K.** Experimental studies on artificial blood usage for hemodilution during cardiopulmonary bypass. *Ann Thorac Cardiovasc Surg* 11: 238–244, 2005.
21. **Ishikura K, Yamada N, Ito M, Ota S, Nakamura M, Isaka N, Nakano T.** Beneficial acute effects of rho-kinase inhibitor in patients with pulmonary arterial hypertension. *Circ J* 70: 174–178, 2006.
22. **Ishizaki T, Uehata M, Tamechika I, Keel J, Nonomura K, Maekawa M, Narumiya S.** Pharmacological properties of Y-27632, a specific inhibitor of rho-associated kinases. *Mol Pharmacol* 57: 976–983, 2000.
23. **Jardim C, Rochitte C, Humbert M, Rubenfeld G, Jasinowodolinski D, Carvalho C, Souza R.** Pulmonary artery distensibility in pulmonary arterial hypertension: an MRI pilot study. *Eur Respir J* 29: 476–481, 2007.
24. **Karau K, Johnson R, Molthen R, Dhyani A, Haworth S, Hanger C, Roerig D, Dawson C.** Microfocal X-ray CT imaging and pulmonary arterial distensibility in excised rat lungs. *Am J Physiol Heart Circ Physiol* 281: H1447–H1457, 2001.
25. **Karau K, Molthen R, Dhyani A, Haworth S, Hanger C, Roerig D, Johnson R, Dawson C.** Pulmonary arterial morphometry from microfocal X-ray computed tomography. *Am J Physiol Heart Circ Physiol* 281: H2747–H2756, 2001.
26. **Kobs RW, Chesler NC.** The mechanobiology of pulmonary vascular remodeling in the congenital absence of eNOS. *Biomech Model Mechanobiol* 5: 217–225, 2006.
27. **Kobs RW, Muvarak NE, Eickhoff JC, Chesler NC.** Linked mechanical and biological aspects of remodeling in mouse pulmonary arteries with hypoxia-induced hypertension. *Am J Physiol Heart Circ Physiol* 288: H1209–H1217, 2005.
28. **Lammers SR, Kao PH, Qi HJ, Hunter K, Lanning C, Albietz J, Hofmeister S, Mecham R, Stenmark KR, Shandas R.** Changes in the structure-function relationship of elastin and its impact on the proximal pulmonary arterial mechanics of hypertensive calves. *Am J Physiol Heart Circ Physiol* 295: H1451–H1459, 2008.
29. **Lejeune P, Deloof T, Leeman M, Mélot C, Naeije R.** Multipoint pulmonary vascular pressure/flow relationships in hypoxic and in normoxic dogs: effects of nitrous oxide with and without cyclooxygenase inhibition. *Anesthesiology* 68: 92–99, 1988.
30. **Li F, Xia W, Yuan S, Sun R.** Acute inhibition of Rho-kinase attenuates pulmonary hypertension in patients with congenital heart disease. *Pediatr Cardiol* 30: 363–366, 2009.
31. **Linehan J, Haworth S, Nelin L, Krenz G, Dawson C.** A simple distensible vessel model for interpreting pulmonary vascular pressure-flow curves. *J Appl Physiol* 73: 987–994, 1992.
32. **Mahapatra S, Nishimura R, Sorajja P, Cha S, McGoon M.** Relationship of pulmonary arterial capacitance and mortality in idiopathic pulmonary arterial hypertension. *J Am Coll Cardiol* 47: 799–803, 2006.
33. **Mathers J, Benumof J, Wahrenbrock E.** General anesthetics and regional hypoxic pulmonary vasoconstriction. *Anesthesiology* 46: 111–114, 1977.
34. **McLaughlin V, Archer S, Badesch D, Barst R, Farber H, Lindner J, Mathier M, McGoon M, Park M, Rosenson R, Rubin L, Tapson V, Varga J.** ACCF/AHA 2009 expert consensus document on pulmonary hypertension a report of the American College of Cardiology Foundation Task Force on Expert Consensus Documents and the American Heart Association developed in collaboration with the American College of Chest Physicians; American Thoracic Society,; and the Pulmonary Hypertension Association. *J Am Coll Cardiol* 53: 1573–1619, 2009.
35. **McMurtry I, Abe K, Ota H, Fagan K, Oka M.** Rho kinase-mediated vasoconstriction in pulmonary hypertension. *Adv Exp Med Biol* 661: 299–308, 2010.
36. **Merklinger SL, Wagner RA, Spiekerkoetter E, Hinek A, Knutsen RH, Kabir MG, Desai K, Hacker S, Wang L, Cann GM, Ambartsumian NS, Lukanidin E, Bernstein D, Husain M, Mecham RP, Starcher B, Yanagisawa H, Rabinovitch M.** Increased fibulin-5 and elastin in S100A4/Mts1 mice with pulmonary hypertension. *Circ Res* 97: 596–604, 2005.
37. **Meyrick B, Reid L.** Pulmonary hypertension. Anatomic and physiologic correlates. *Clin Chest Med* 4: 199–217, 1983.
38. **Milnor WR.** *Hemodynamics*. Baltimore, MD: Williams and Wilkins, 1989, p. 419.
39. **Molthen RC, Karau KL, Dawson CA.** Quantitative models of the rat pulmonary arterial tree morphometry applied to hypoxia-induced arterial remodeling. *J Appl Physiol* 97: 2372–2384, 2004.
40. **Mortimer H, Peacock A, Kirk A, Welsh D.** p38 MAP kinase: essential role in hypoxia-mediated human pulmonary artery fibroblast proliferation. *Pulm Pharmacol Ther* 20: 718–725, 2007.
41. **Naeije R.** Pulmonary vascular function. In: *Pulmonary Circulation: Diseases and Their Treatment*, edited by Peacock AJ and Rubin LJ. London: Arnold, 2004, p. 3–11.
42. **Nagaoka T, Fagan KA, Gebb SA, Morris KG, Suzuki T, Shimokawa H, McMurtry IF, Oka M.** Inhaled Rho kinase inhibitors are potent and selective vasodilators in rat pulmonary hypertension. *Am J Respir Crit Care Med* 171: 494–499, 2005.
43. **Nagaoka T, Morio Y, Casanova N, Bauer N, Gebb S, McMurtry I, Oka M.** Rho/Rho kinase signaling mediates increased basal pulmonary vascular tone in chronically hypoxic rats. *Am J Physiol Lung Cell Mol Physiol* 287: L665–L672, 2004.
44. **Nichols WW, O'Rourke MF, Hartley C, McDonald DA.** *McDonald's Blood Flow in Arteries: Theoretical, Experimental, and Clinical Principles*. London: Arnold, 2005.
45. **O'Flynn P, O'Sullivan G, Pandit A.** Geometric variability of the abdominal aorta and its major peripheral branches. *Ann Biomed Eng* 38: 824–840, 2010.
46. **Oka M, Homma N, Taraseviciene-Stewart L, Morris K, Kraskauskas D, Burns N, Voelkel N, McMurtry I.** Rho kinase-mediated vasoconstriction is important in severe occlusive pulmonary arterial hypertension in rats. *Circ Res* 100: 923–929, 2007.
47. **Phan S.** The myofibroblast in pulmonary fibrosis. *Chest* 122: 286S–289S, 2002.
48. **Rabinovitch M, Gamble W, Nadas AS, Miettinen OS, Reid L.** Rat pulmonary circulation after chronic hypoxia: hemodynamic and structural features. *Am J Physiol Heart Circ Physiol* 236: H818–H827, 1979.
49. **Saeed M, Hartmann A, Bing R.** Inhibition of vasoactive agents by perfluorochemical emulsion. *Life Sci* 40: 1971–1979, 1987.

50. **Sanz J, Kariisa M, Dellegrottaglie S, Prat-González S, Garcia M, Fuster V, Rajagopalan S.** Evaluation of pulmonary artery stiffness in pulmonary hypertension with cardiac magnetic resonance. *JACC Cardiovasc Imaging* 2: 286–295, 2009.
51. **Schwenke D, Pearson J, Kangawa K, Umetani K, Shirai M.** Changes in macrovessel pulmonary blood flow distribution following chronic hypoxia: assessed using synchrotron radiation microangiography. *J Appl Physiol* 104: 88–96, 2008.
52. **Schwenke D, Pearson J, Umetani K, Kangawa K, Shirai M.** Imaging of the pulmonary circulation in the closed-chest rat using synchrotron radiation microangiography. *J Appl Physiol* 102: 787–793, 2007.
53. **Stenmark K, Meyrick B, Galie N, Mooi W, McMurtry I.** Animal models of pulmonary arterial hypertension: the hope for etiological discovery and pharmacological cure. *Am J Physiol Lung Cell Mol Physiol* 297: L1013–L1032, 2009.
54. **Stenmark KR, Fagan KA, Frid MG.** Hypoxia-induced pulmonary vascular remodeling: cellular and molecular mechanisms. *Circ Res* 99: 675–691, 2006.
55. **Stenmark KR, McMurtry IF.** Vascular remodeling versus vasoconstriction in chronic hypoxic pulmonary hypertension: a time for reappraisal? *Circ Res* 97: 95–98, 2005.
56. **Tabima D, Chesler N.** The effects of vasoactivity and hypoxic pulmonary hypertension on extralobar pulmonary artery biomechanics. *J Biomech* 43: 1864–1869, 2010.
57. **Tada Y, Laudi S, Harral J, Carr M, Ivester C, Tanabe N, Takiguchi Y, Tatsumi K, Kuriyama T, Nichols W, West J.** Murine pulmonary response to chronic hypoxia is strain specific. *Exp Lung Res* 34: 313–323, 2008.
58. **Tuchscherer HA, Vanderpool RR, Chesler NC.** Pulmonary vascular remodeling in isolated mouse lungs: effects on pulsatile pressure-flow relationships. *J Biomech* 40: 993–1001, 2007.
59. **Tuchscherer HA, Webster EB, Chesler NC.** Pulmonary vascular resistance and impedance in isolated mouse lungs: effects of pulmonary emboli. *Ann Biomed Eng* 34: 660–668, 2006.
60. **Vanderpool RR, Naeije R, Chesler NC.** Impedance in isolated mouse lungs for the determination of site of action of vasoactive agents and disease. *Ann Biomed Eng* 38: 1854–1861, 2010.
61. **Voelkel N, Quaife R, Leinwand L, Barst R, McGoon M, Meldrum D, Dupuis J, Long C, Rubin L, Smart F, Suzuki Y, Gladwin M, Denholm E, Gail D.** Right ventricular function and failure: report of a National Heart, Lung, and Blood Institute working group on cellular and molecular mechanisms of right heart failure. *Circulation* 114: 1883–1891, 2006.
62. **Von Bethmann AN, Brasch F, Nusing R, Vogt K, Volk HD, Muller KM, Wendel A, Uhlig S.** Hyperventilation induces release of cytokines from perfused mouse lung. *Am J Respir Crit Care Med* 157: 263–272, 1998.
63. **Westerhof N, Stergiopulos N, Noble MIM.** *Snapshots of Hemodynamics An Aid for Clinical Research and Graduate Education*. New York: Springer, 2004, p. 192.
64. **Yen R, Zhuang F, Fung Y, Ho H, Tremer H, Sobin S.** Morphometry of cat's pulmonary arterial tree. *J Biomech Eng* 106: 131–136, 1984.
65. **Zhao J, Day J, Yuan Z, Gregersen H.** Regional arterial stress-strain distributions referenced to the zero-stress state in the rat. *Am J Physiol Heart Circ Physiol* 282: H622–H629, 2002.